Protein Transport through a Narrow Solid-State Nanopore at High Voltage: Experiments and Theory

Benjamin Cressiot,[†] Abdelghani Oukhaled,[†] Gilles Patriarche,[§] Manuela Pastoriza-Gallego,[†] Jean-Michel Betton,[⊥] Loïc Auvray,[∥] Murugappan Muthukumar,[‡] Laurent Bacri,[†] and Juan Pelta[†,*]

[†]LAMBE UMR CNRS 8587, Université d'Evry et de Cergy-Pontoise, France, [‡]Department of Polymer Science and Engineering, University of Massachusetts, Amherst, Massachusetts 01003, United States, [§]LPN/CNRS, Marcoussis, France, [⊥]Unité de Biochimie Structurale, Institut Pasteur, France, and [∥]Matière et Systèmes Complexes, UMR CNRS 7057, Université Paris Diderot, France

ABSTRACT

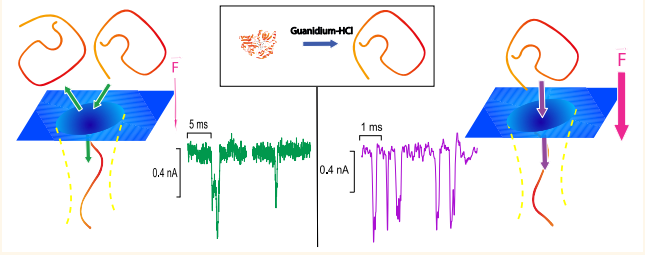

We report experimentally the transport of an unfolded protein through a narrow solid-state nanopore of 3 nm diameter as a function of applied voltage. The random coil polypeptide chain is larger than the nanopore. The event frequency dependency of current blockades from 200 to 750 mV follows a van't Hoff–Arrhenius law due to the confinement of the unfolded chain. The protein is an extended conformation inside the pore at high voltage. We observe that the protein dwell time decreases exponentially at medium voltage and is inversely proportional to voltage for higher values. This is consistent with the translocation mechanism where the protein is confined in the pore, creating an entropic barrier, followed by electrophoretic transport. We compare these results to our previous work with a larger pore of 20 nm diameter. Our data suggest that electro-osmotic flow and protein adsorption on the narrowest nanopore wall are minimized. We discuss the experimental data obtained as compared with recent theory for the polyelectrolyte translocation process. This theory reproduces clearly the experimental crossover between the entropic barrier regime with medium voltage and the electrophoretic regime with higher voltage.

KEYWORDS: solid-state nanopore · transmission electron microscope · protein translocation · protein unfolding · Fokker–Planck model

Nanopores are very promising in the field of macromolecule manipulation at the single-molecule level.[1−5] One of the most common potential applications is ultrafast DNA or RNA sequencing.[6] For the past few years, it has also been possible to use protein or solid-state nanopores as protein conformation sensors. We propose possible applications using nanopores with electric detection (the sequencing of proteins, assisted protein folding) to detect mutation and misfolding. All these applications could be performed subject to precise control of the pore size, which must be smaller than the protein, and also the driving force to control the transport velocity.

Protein trafficking through channels plays an important role in many biological processes.[7] An excellent technique probing the dynamics of protein conducting channels[8] at the single-molecule level is the bilayer lipid membrane technique used in the context of protein transport for mitochondrial pores[9,10] and translocon machinery.[11] The translocon, an active transmembrane protein channel,[12] allows protein translocation in a cell assisted by a peripheral attached protein motor powered by ATP hydrolysis. The translocation is associated with either protein synthesis (co-translation) or after protein synthesis (post-translation). After transport, proteins need to be correctly folded to be functional. In order to understand this mechanism, it is easier to perform protein transport experiments through protein channels or solid-state nanopores by substituting the ATP energy by an electric force. An applied electric field drives a macromolecule into the nanopore, inducing transient blockades of electrical current and a measurable decrease in conductance.[3,13] The current blockade duration and rate depend on the size and conformation of the passing macromolecule, the diameter and the length of the protein pore or solid-state nanopore, and the interaction between the molecule and the pore walls.

Up to now, various studies have been carried out using protein channels. It is possible to probe protein unfolding transitions with a denaturing agent,[1,14] with thermal denaturation,[15] or using an electric field[16] and protein

* Address correspondence to juan.pelta@u-cergy.fr.

Received for review April 16, 2012 and accepted June 6, 2012.

Published online June 06, 2012
10.1021/nn301672g

folding with cationic ions.[16,17] The structures of peptides were also investigated through protein nanopores.[18−20] Interactions between proteins and channels[21] and recently the transport dynamics through toxin channels[22,23] or through a mitochondrial channel[24] have been investigated. Nevertheless, these pores are sensitive to high denaturing agent concentrations,[23,25,26] and their lifetime is short (a few hours) due to the fragility of the lipid membrane. Solid-state nanopores have the advantage of being insensitive to these high concentrations of denaturing agent with a longer lifetime (several days) and to high electric driving forces. On the other hand, it remains difficult to create solid-state nanopores with high reproducibility in terms of shape. Furthermore, the transport dynamics are not easily controlled due to the protein−nanopore interactions[27] and/or electro-osmotic flow.[28]

Solid-state nanopores have been used as an electrical detector of native or partially unfolded proteins.[29−34] A demonstration of BSA protein translocation through a solid-state nanopore has already been performed by chemiluminescent analysis.[35] Solid-state nanopores have also been used for the study of anomalous transport in the case of protein−protein interactions,[32,36,37] protein−nanopore wall interactions,[27] and the effect of electro-osmosis on the dynamics of protein transport.[28] Recently, solid-state nanopores have been coated with a fluid lipid bilayer containing mobile ligands attached to the surface. This made it possible to differentiate proteins by current blockage analysis and slow the dynamics of protein transport.[29] Metalized silicon nitride nanopores, chemically modified with receptors, are used to detect subclasses of IgG antibodies.[34] Some theoretical works and simulations have also been performed on protein translocation.[38−40]

The protein model in our study is the maltose binding protein (MalE),[41] composed of 51 acidic residues (24 Asp +27 Glu) and 43 basic residues (37 Lys +6 Arg), uniformly distributed along the primary sequence. Its pI is 5.2; thus the protein is negatively charged at pH 7.5, and the protein net charge is −8*e*. From the 3D structure, there is no visible cluster of charged residues; therefore we assumed that charged residues are also uniformly distributed in the unfolded conformations. In our experimental conditions the unfolded proteins have a random coil conformation in the presence of denaturing agent and high salt concentration. The diameter of the flexible polypeptide chain is around 8 nm. We have already studied the dynamic properties of the entry and transport of unfolded and folded maltose binding protein (MBP, MalEwt), through a 20 nm solid-state nanopore performed by focused ion beam (FIB) as a function of applied voltage between 25 and 250 mV. The pore diameter is larger than the folded and unfolded protein size.[42] We showed that these dynamics are associated with a high free-energy barrier probably associated with protein−nanopore wall adsorption. In the presence of proteins, the event frequency of current blockades increases exponentially as a function of applied voltage. At medium electrical force, we observe frequency saturation for unfolded proteins. We have observed that the current blockade durations of the folded and unfolded proteins decrease exponentially as the applied electric field increases. In our experimental conditions, the electro-osmotic flow is in the opposite direction of the electric driving force. The dwell time of proteins (current blockade) dependency showed us that the electro-osmotic flow is not dominant for the dynamics of protein transport. These times are found anomalously long in comparison to expected dwell times based on the electrophoretic mobility; they are probably mainly due to protein−pore interactions. In order to obtain better insight into our previous work, experiments are driven with a 3 nm solid-state nanopore created using TEM, the unfolded protein MBP being at least three times larger than the nanopore diameter. Consequently, the transported protein would be in an extended conformation. This pore diameter is similar to the diameter of the biological channels involved in the translocation of unfolded proteins. To be sure that the unfolded proteins are really transported by an electrophoretic mechanism through the nanopore, we applied high voltages (from 200 to 750 mV). The electro-osmotic velocity is controlled by the geometry, the diameter, the net charge of the pore, the ionic strength, and the pH of solution.[28,43−46] Here, the Debye length remains on the same order as previous experiments using the large pores. We also use the same solid-state membrane (Si_3N_4), but the large pores were drilled by using FIB techniques and the narrow ones by TEM techniques. We can suppose that, in the first case, the nanopores contain some gallium ions, while, in the second case, the charges are annealed by the electron beam.[47] This phenomenon could explain the linear *I*−*V* curve observed with nanopores drilled by TEM, in agreement with Schulten's recent work.[47] The differences are a strong decrease of the nanopore diameter and the net charge of the nanopore (the solution pH does not change). We expect an increase of electro-osmotic velocity of the fluid due to a decrease of the pore diameter and a decrease of the electro-osmotic flow due to the net charge decrease.[46]

Moreover, independently of the hydrodynamic effects, the confinement becomes more important, and the energetic penalty becomes higher to enter the narrow pore. In any case, one expects that the protein dynamics and frequency should slow dramatically. Surprisingly, we observe shorter dwell times and higher event frequency. The experimental entry of molecules as a function of electric driving force follows an exponential dependency. The transport is dominated by either the free-energy barrier or the electrophoretic mechanism in the medium or high-voltage regime, respectively, consistent with the entropic barrier

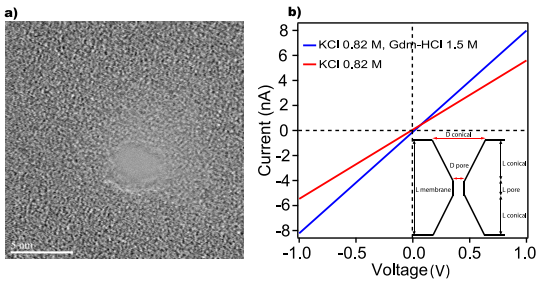

Figure 1. Transmission electronic microscopy (TEM) nanopore fabrication for the transport of unfolded proteins. (a) Bright field (BF) STEM image of a 3 nm diameter solid-state nanopore performed in a 30 nm thick Si_3N_4 membrane. (b) *I*/*V* characteristic curve through a solid-state nanopore in 0.82 M KCl and 5 mM Hepes pH 7.5 and in the presence of 1.5 M Gdm-HCl. The inset shows the geometry of the pore.

mechanism of polymer translocation. The event frequency is 10 times higher and the activation energy is three times lower with the 3 nm pore than with the previous 20 nm pore. Our results suggest that electroosmotic flow and protein adsorption on the nanopore wall should be minimized. Therefore, it is possible to control protein transport through a narrow pore at high voltage. In this work, we attempt to enhance the understanding of protein transport through a small nanopore. Data are discussed according to a theory of capture rates in polyelectrolyte transport through narrow nanopores.[48] It has been shown that the process of polyelectrolyte capture by the nanopore under an electric field is delineated by two regimes: an entropic barrier regime and a drift regime. In the first regime dominated by the entropic barrier for the polyelectrolyte, at medium voltage differences, the capture rate is an increasing nonlinear function in the electric field. In the drift regime, where the electric driving force dwarfs the role of entropic barriers, at higher applied voltages, the capture rate is linear in the electric field.

RESULTS AND DISCUSSION

Figure 1a shows a bright-field (BF) STEM image of a 3 nm diameter solid-state nanopore drilled in a 30 nm thick Si_3N_4 membrane. From this picture, we measure the pore diameter: d_{pore} = 3 ± 0.15 nm (Supporting Information). Figure 1b shows the current−voltage (*I*−*V*) characteristics through a 3 nm solid-state nanopore in 0.82 M KCl (red curve, σ = 9 S/m) and 0.82 M KCl + 1.5 M guanidium-HCl (blue curve, σ = 12.6 S/m) buffer. A linear fit to the data yields conductance values of 5.5 and 8.1 nS in 0.82 M KCl and 0.82 M KCl + 1.5 M Gdm-HCl, respectively. The denaturing agent (guanidium-HCl) does not affect either the noise level or the pore stability. Addition of guanidium-HCl just increases the open pore level (*i.e.*, the pore conductance G_{pore}) by about 40%. Note that in both cases, the *I*−*V* characteristics are linear,[47,49−51] in contrast with our previous works on pores drilled by FIB[42,52] or asymmetrical conical pores in polymer membranes,[53] where current asymmetry was usually observed.

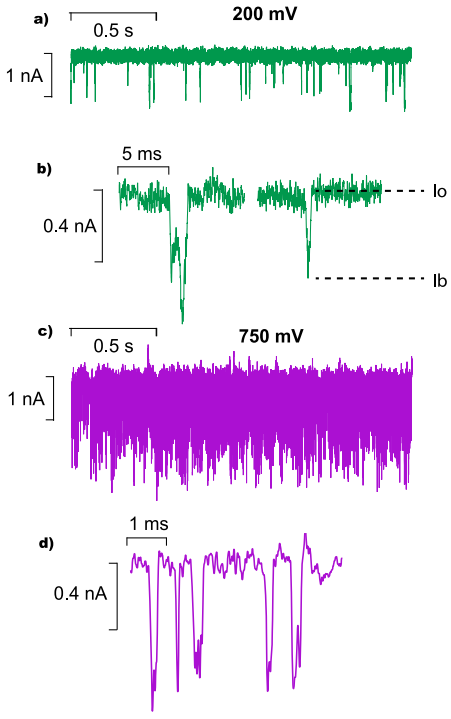

Figure 2. Detail of current trace recording in the presence of unfolded MBP protein. The protein concentration is 10.4 μM in a 0.82 M KCl and 5 mM Hepes, pH 7.5, buffer. To unfold the MBP, the experiment was performed in 1.5 M guanidium chloride. Individual events are shown with increased time resolution for each transmembrane potential. (a) Current traces at a transmembrane potential of 200 mV. We observe two types of events: one short with low-magnitude current blockade (on the right) and one longer and deeper (on the left) (b), I_0 is the average current of the baseline, I_b the mean current of each event. Current traces at a transmembrane potential of 750 mV (c). We observe only one type of events (d).

Using a simplified model where the nanopore is approximated by two cones and a cylinder[54] (inset of Figure 1b), the conductance of the conical part is $G_{conical} = (\pi\sigma/4)d_{pore}(d_{conical}/L_{conical})$, where $d_{conical}$ is the diameter and $L_{conical}$ is the height of the cone. The cylinder conductance is $G_{cylinder} = (\pi\sigma/4)(d_{pore}^2/L_{pore})$. The access conductance is $G_{access} = 2d_{pore}\sigma$.[55] The total conductance can be written as $1/G_{pore} = 2(1/G_{conical}) + 1/G_{cylinder} + 1/G_{access}$. Taking into account that $L_{membrane} = (2L_{conical} + L_{pore})$ where $L_{membrane}$ is the membrane thickness, we evaluate an effective pore length L_{pore}= 4.9 ± 1.4 nm (Supporting Information). Note that the *I*−*V* characteristics obtained from the 3 nm solid-state nanopore after immersion in PEG solutions are not altered, suggesting that the apparent pore diameter remains unchanged. This means that the PEGs are not interacting with the pore walls irreversibly (Supporting Information).

Analysis of the Current Blockades and Dwell Times. After the addition of unfolded proteins in the *cis* (negative) compartment, deep current blockades are observed (Figure 2). Details of two current traces at 200 mV (Figure 2a) and 750 mV (Figure 2c) are shown. For each applied voltage we focus on the current traces

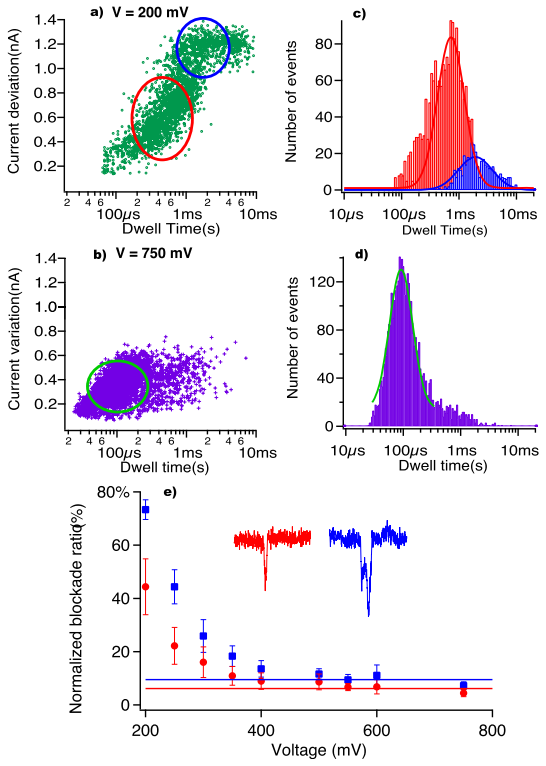

Figure 3. Current variation events of unfolded proteins *versus* applied voltage. Current variation *versus* the dwell time (a, b) and histograms of dwell times (c, d) at two applied voltages, 200 mV (a, c) and 750 mV (b, d). (e) Normalized current blockage ratio $[(I_0 - I_b)/I_0]$ (%) as a function of applied voltage for short (red) and long (blue) events.

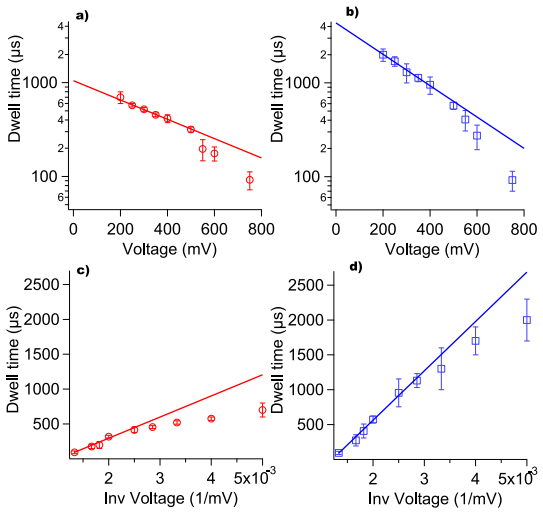

Figure 4. Dwell time of events as a function of transmembrane potential. Dwell time of short (red) (a,c) or long (blue) (b,d) events for unfolded proteins as a function of applied voltage. Between 200 and 400 mV, we find using the equation $f(V) = A\exp(-V/V_0)$, $A_{short} = 1050 \pm 161$ μs, $V_{0short} = 422 \pm 89$ mV and $A_{long} = 4361 \pm 1250$ μs, $V_{0long} = 260 \pm 63$ mV. Between 400 and 750 mV, we find using the equation $f(V) = b/V + a$, $a_{short} = -312 \pm 57$ μs, $b_{short} = 303\,540 \pm 32\,400$ μs·mV and $a_{long} = -855 \pm 107$ μs, $b_{long} = 708\,300 \pm 71\,500$ μs·mV.

(Figures 2b and d, respectively). At low voltages (200 mV) we observe two types of events: one short with a low-magnitude current blockade and the other longer and deeper. At high voltages (750 mV), the durations of both types of events are similar to low-magnitude and short-current blockade events.

In Figure 3a, we observe two populations of events for the current deviation $(I_0 - I_b)$ *versus* the dwell time at 200 mV. The current deviation of the longer events (1.19 ± 0.06 nA) is approximately twice that of the short ones (0.72 ± 0.17 nA). At 750 mV, we observe just one large population of events in Figure 3b.

We then plot the normalized current blockade ratio $[(I_0 - I_b)/I_0]$ (%) as a function of the applied voltage (Figure 3e), where I_0 is the average current of the baseline and I_b the mean current of each event. We observe the same behavior for both short and long events: a strong decrease until 400 mV from 73% down to 13% for long events and from 44% to 9% for short events. For voltages higher than 400 mV, the ratio reaches a constant value (6.1 ± 2.3% for short events and 9.5 ± 2.5% for long events). This means that unfolded protein is stretched as a function of electric driving force up to 400 mV, and when the applied voltage increases even more, the extended conformation does not change inside the narrow pore.

We assume that above 400 mV the chain is fully extended inside the narrowest region approximated by a cylindrical shape, with an effective length $L_{pore} = 4.9 \pm 1.4$ nm and a radius $r_{pore} = 1.5 \pm 0.08$ nm. For an unfolded protein, the unit segment is the persistence length. It is natural to choose a cylinder for the molecule geometry, $r_{monomer} = 0.33 \pm 0.02$ nm (size of one amino acid). The predicted volume occupied by the extended portion of protein passing through the pore effective length is given by the volume of the protein V_{prot} divided by the volume of the pore V_{pore}: $V_{prot}/V_{pore} = r_{monomer}^2/r_{pore}^2 = 5 \pm 1\%$. This result is in agreement with the experimental value of the normalized current blockade ratio $[(I_0 - I_b)/I_0]$ at the plateau (9.5 ± 2.5%). In fact, this estimation shows that the chain is completely stretched in the pore.

We could suppose that short events are described by one protein entering the pore, and longer events by two proteins entering in single file.[56] To check this hypothesis, we can look at the dwell time behavior. Histograms of the dwell times presented in Figure 3 give us the time distribution for each applied voltage. The maximum of this distribution defines the most probable dwell time. At 200 mV (Figure 3c), the characteristic time for short events with low-magnitude current blockade is 700 ± 100 μs, while for longer and deeper events this time is 2000 ± 300 μs. At high voltage (750 mV) there is only one large distribution (Figure 3d), which is like the short one observed at medium voltage (200 mV).

We expect two dynamics inside the nanopore; the first one is described by an energy barrier. We expect

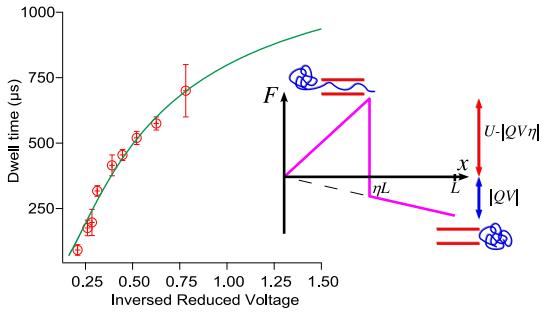

Figure 5. Comparison between theoretical translocation time and experimental dwell time *versus* reciprocal of dimensionless voltage corresponding to the experiment (left). Sketch of the free-energy landscape (right). The average modelized translocation time is plotted (green curve) against 1/*v*, $v = |QV|$ in units of k_BT, for the experimental range of voltage, *V*, from 200 to 800 mV, experimental data (red markers). The experimental effective charge of the protein is $Q = -0.16e$ and the pore length is *L*; we obtain the energy barrier, $U = (9 \pm 1.4)k_BT$, and the barrier location $\eta = 0.54 \pm 0.03$. The free-energy profile permits explaining the crossover from an exponential dependence of the residence time at moderate voltages to the inverse voltage dependence at higher voltages.

an exponential dependency of the transport time as a function of the applied voltage. The second one is described by an electrophoretic transport,[52] and the translocation time is expected to be inversely proportional to the applied force. We represent the blockade times as a function of the applied voltage (Figure 4) for short and long events. The blockade duration decreases in both cases as the applied electric field increases. We have examined both hypotheses: in our case, the exponential fit is the best one at medium voltages smaller than 400 mV, so a model of an activation barrier is better (Figure 4), which could be explained by protein−pore nonspecific interactions. For voltages higher than 400 mV, the behaviors follow electrophoretic dynamics (Figure 4). At high electric driving force, the protein is transported through the nanopore.

In order to understand the crossover from an exponential dependence of the residence time at moderate voltages to the inverse voltage dependence at higher voltages, we have considered a free-energy profile (inset in Figure 5) along the translocation direction, where there exists a barrier *U* followed by a ramp due to the electric field across the pore. The barrier arises from the confinement of the polymer at the pore entry initially without grafting between the chain end and the pore mouth. The chain end must unravel from its initial confined state to place itself at the pore entry, which results in an entropic barrier. The barrier is assumed to be present at a distance of ηL, where *L* is the pore length. In addition to the entropic barrier there is a potential energy drop of $|QV|$ across the pore. Although the free-energy profile across the pore could be more complicated, we take the simplest profile to gain an understanding of the most dominant factor responsible for the crossover. For the free-energy landscape[48,57,58] of Figure 5, the average translocation time τ follows from the Fokker−Planck formalism as

$$\tau(v) \propto \frac{\eta}{(u - v\eta)}(e^{u - v\eta} - 1) - \frac{1}{v}(e^{-v} - e^{-v\eta})$$

(See Supporting Information.) Here η is the location of the barrier, and $v = |QV|$. *u* and *v* are in units of k_BT. Taking the experimental charge of the protein to be $Q = -0.16e$ (see below), we fit the measured dwelling times plot and we calculate the values for $U = 9 \pm 1.4\ k_BT$ and for $\eta = 0.54 \pm 0.03$. A plot of the modelized translocation time τ against $(1/v)$ as well as the experimental data is presented in Figure 5. The model reproduces clearly the experimental crossover.

Surprisingly, the measured dwell time through a 3 nm (t_{3nm}) pore is comparable with that measured through a 20 nm (t_{20nm}) pore[42] at the same applied voltage. Because of confinement effects, one would expect to measure longer times. If we consider a purely diffusive transport[59] through a long pore, the dwell time *t* is $t = L^2\eta_0 Na/k_BT(a/D)^{2/3}$, *L* being the pore length, η_0 the solution viscosity, *N* the monomer number, *a* the monomer size, *D* the pore diameter, and k_BT the thermal energy. Comparing t_{3nm} to t_{20nm}, we find $t_{3nm} = t_{20nm}(D_{20nm}/D_{3nm})^{2/3} \cong 7^{2/3}t_{20nm}$, while we find in our measurement, $t_{3nm} \cong t_{20nm}$ (700 ± 100 μs). The unfolded protein transport dynamics through the two pores are different according to a scaling argument. In our previous work, we explained these long times by two phenomena: either electro-osmotic flow due to the charged surface of the nanopore wall, or protein attractive interactions with the nanopore wall. In the case of electro-osmotic flow, it was observed previously by Wanunu *et al.*[60] that the event frequency decreased when the applied electric force increased. In order to check the importance of electro-osmotic flow in this study, we performed an experiment with neutral polymers as a function of electric field (Supporting Information). The event frequency and the dwell time of PEG transport as a function of the applied voltage remain constant. The current deviation follows Ohm's law behavior as a function of the applied voltage. These results show that electro-osmotic flow is greatly reduced in our experimental conditions. A recent simulation work predicts that the interactions between protein and nanopore could be strong for FIB nanopores, due to gallium ions, and weak for TEM nanopores, because the silica surface rearranges and the patches of dangling atoms are removed.[47] The interactions between the protein and the pore wall could be weak; this is a possible explanation of our observation of translocation times being shorter than expected. Nevertheless, this time remains long compared to that predicted in the absence of interaction, which is on the order of a microsecond.[32] This is quite a common

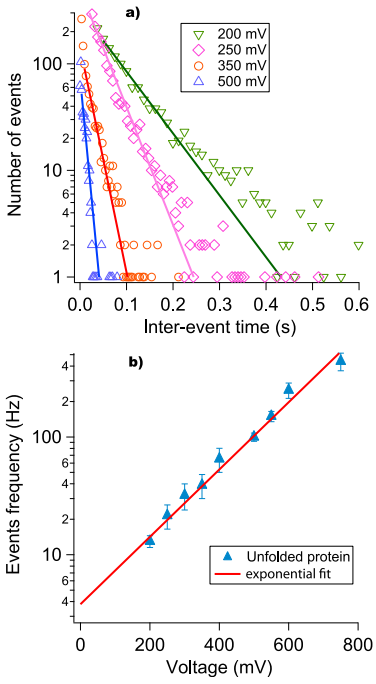

Figure 6. Frequency of current blockades *versus* applied voltage in semilog scale. (a) Explanation of the statistical analysis of the measured current traces, distribution of inter-event intervals T_i for four different applied voltages. (b) Frequency of events *versus* applied voltage. The red line is an exponential fit of equation $f = f_0 \exp(|V|/V_0)$ with $f_0 = 3.8 \pm 0.5$ Hz and $V_0 = 152 \pm 6.4$ mV.

phenomenon, particularly on such a high-energy surface as that of SiN,[61] and many authors[27,30,42] give prominence to it.

Analysis of Event Frequency. From the inter-event duration histogram (Figure 6a), we observe that the blockade current frequency increases exponentially as the applied voltage increases from 200 mV to 750 mV (Figure 6b). We use a van't Hoff Arrhenius formalism, $R = R_0 \exp(|V|/V_0)$, where $R_0 \alpha f^* \exp(-U^*/k_BT)$ is the zero voltage capture rate controlled by an activation barrier U^* (f^* is a frequency factor) of entropic and electrostatic origin. The ratio $|V|/V_0 = (zeV)/k_BT$ is a barrier reduction factor due to the applied voltage V, acting on ze, the effective electric charge of the molecule, where z is the magnitude of the effective total number of elementary charges of the protein, e is the elementary charge, and k_BT is the thermal energy. The potential V_0 ($V_0 = k_BT/ze$) corresponds to the necessary applied potential to allow a charged protein to overcome the Brownian motion. Frequency data are well described by an exponential fit of the equation $f = f_0 \exp(|V|/V_0)$, where $f_0 = 3.8 \pm 0.5$ Hz and $V_0 = 152 \pm 6.4$ mV.

The protein net charge is $-8e$ in solution in the absence of counterion condensation. The effective charge z is extracted from indirect measurement $z = (k_BT)/(V_0e) = 0.16 \pm 0.01$.

Up to now, we have just qualitative possible explanations to discuss the high charge reduction at the entry of the nanopore. The reduction of unfolded protein charge could be due to the charge confinement in the medium of low dielectric constant[62] or to back-flow effects.[28,45,63]

In order to estimate the activation energy, we calculate the frequency factor (f^*) from the barrier penetration calculation $f^* = CD_{diff}A_{pore}/L_{pore}$, where $C = 6.24 \times 10^{21}$ molecules/m^3 is the bulk concentration of MBP protein (corresponding to $c = 10.4$ μM), $D_{diff} = 10^{-10}$ m^2/s is its diffusion coefficient, $A_{pore} = \pi 10^{-18}$ m^2 is the cross-sectional area of the pore, and $L_{pore} = 4.9 \pm 1.4$ nm is the pore length. We find $U^* \approx (4.2 \pm 0.5)k_BT$ for just the entry of an unfolded protein. If we consider both the protein capture and the chain confinement inside the pore, we obtain $U = (9 \pm 1.4)k_BT$ (Figure 5).

We expected an increase of the energy barrier by a factor $(D_{20nm}/D_{3nm})^{5/3} \approx 24$ if we consider that the entropic barrier is dominated by the confinement of the chain.[64,65] However, this energy barrier is two times smaller than that obtained with the 20 nm pore ($U^* \approx 10.4k_BT$). This means that either electrostatic or hydrophobic interactions could contribute to this activation energy. We have previously determined the activation energy for the entry of unfolded proteins through protein pores. We obtained $U^* \approx 2k_BT$ for the alpha-hemolysin and $U^* \approx 4k_BT$ for the aerolysin. These pores have a similar diameter to the solid-state one (around 2 nm), but their net charge is different. For these protein nanopores, the entropy is the major contribution for unfolded protein pore entrance.[14,23] We expected an entropic penalty for an excluded volume chain of a neutral polymer: $U^* \approx (L_{pore}/D)k_BT \approx (1.6 \pm 0.4)k_BT$.[40] In our experimental conditions, the high salt concentration screens the electrostatic interactions. Finally, the main contribution in our experiments for protein entrance with a narrow solid-state nanopore is an entropic barrier.

CONCLUSION

In conclusion, we compare the transport of unfolded proteins as a function of the applied voltage (from 200 to 750 mV) through a 3 nm solid-state nanopore drilled by TEM to our previous work with a 20 nm solid state nanopore drilled by FIB. We observe surprisingly for the narrowest pore a higher event frequency, a lower activation energy, and shorter times than expected. We show that the entry of unfolded proteins inside the narrow nanopore is dominated by the entropic effect associated with the confinement of the chains. The protein is progressively stretched under the applied voltage and assumes an extended conformation at high voltages. The dwell time decreases exponentially at medium voltage: the chains interact with the nanopore walls and escape from the pore. This time is inversely proportional to the applied force at high voltage: the unfolded proteins are really transported through the pore by an electrophoretic mechanism. The theoretical model fits well the results and the experimental crossover. There

are two steps during translocation: (I) capture of the chain to fill the pore; (II) transfer while keeping the pore filled. This model has an exponential behavior at medium voltages and linear dependence at higher voltages; the free-energy barrier and the location of the barrier are the adjustable parameters.

METHODS

Nanopores. The nanoholes were manufactured using a TEM/STEM Jeol 2200FS microscope operating at 200 keV and equipped with an aberration corrector on the probe (STEM mode). The nano-openings were created using a 1.3 nA electron probe, a half-convergence angle of 30 mrad, and a spot size (fwhm) of 0.4 nm. The width of the scanning window determines the size of the nano-opening. The etching process is observed *in situ* and stopped when the nanohole is formed in the scanning window. The post-treatment observations in high-angle annular dark field imaging mode are performed using a lower energy probe (240 pA and a spot size of 0.15 nm) to avoid any modification of the shape of the hole.

All of the nanopores were adapted to an easy-to-use "Port-a-Patch" setup (Nanion Technologies Gmbh). They were glued onto a drilled screw cap containing a 1−2 mm wide hole. This chip can be easily handled and rinsed with water and ethanol. In order to make the membrane hydrophilic, we cleaned this chip by exposing each side to oxygen plasma for 2 min. We then applied a 10 μL buffer droplet to each side of the nanopore using a micropipet. The buffer was an ionic solution of 0.82 M KCl containing 5 mM Tris (pH 7.5) and allowed good storage conditions. The experiments were conducted in a water-saturated atmosphere. The effective pore diameter was deduced from an open-pore conductance measurement. The denaturing agent (guanidium-HCl) did not affect the noise level or the pore stability. The addition of guanidium-HCl only increased the ionic current of the open pore.

Proteins. The recombinant maltose binding protein (MBP or MalEwt) of *Escherichia coli* contained 370 residues ($M_r = 40\,707$) and was negatively charged (with a net charge $Z = -8e$) at physiological pH. The wild-type MBP was purified as described.[66] The buffer was an ionic solution of 0.82 M KCl containing 5 mM Tris (pH 7.5). In this study, we added to this ionic solution the recombinant MBP denatured by guanidium chloride (Gdm-HCl), the final concentration of guanidium chloride being 1.5 M.

Data Acquisition. The ionic currents were detected using an Axopatch 200B amplifier (Molecular Devices). They were first filtered at 10 kHz before a digitization at 250 kHz (4 μs). The data were processed with a homemade macro, using Igor software (Wavemetrics). The event measurements were based on a statistical analysis of the current traces described in a previous article.[67] This method was based on a two-threshold method in the case of events with an asymmetric shape; the event duration was a function of the threshold. Because our threshold criterion was always the same, the measurement error was constant and remained low. All data were obtained with a single nanopore, but for each experimental condition, we measured at least 2000 events. The same nanopore was used during several experiments and several days with the protein. The physical parameters were estimated without the standard deviation between different pores but with the standard deviation of several assays with the same pore. Data were systematically checked for reproducibility.

Conflict of Interest: The authors declare no competing financial interest.

Acknowledgment. This work was supported by grant funding, Action Thématique Incitative Génopole, ANR Blanche "TRANSFOLDPROT" BLAN08-1_339991, and Nanoscience Eranet, ANR "NANOPORE" No. 08-NSCI-006-01. We are grateful to Kari and Damien Foster for their attention to our manuscript and for kindly correcting the language of the manuscript. M.M. acknowledges support from NSF Grant No. DMR1104362.

Supporting Information Available: This material is available free of charge *via* the Internet at http://pubs.acs.org.

REFERENCES AND NOTES

1. Dekker, C. Solid-State Nanopores. *Nat. Nanotechnol.* **2007**, *2*, 209–215.
2. Howorka, S.; Siwy, Z. Nanopore Analytics: Sensing of Single Molecules. *Chem. Soc. Rev.* **2009**, *38*, 2360.
3. Kasianowicz, J. J.; Brandin, E.; Branton, D.; Deamer, D. W. Characterization of Individual Polynucleotide Molecules Using a Membrane Channel. *Proc. Natl. Acad. Sci. U. S. A.* **1996**, *93*, 13770–13773.
4. Movileanu, L. Interrogating Single Proteins through Nanopores: Challenges and Opportunities. *Trends Biotechnol.* **2009**, *27*, 333–341.
5. Muthukumar, M. Mechanism of DNA Transport through Pores. *Annu. Rev. Biophys. Biomol. Struct.* **2007**, *36*, 435–450.
6. Branton, D.; Deamer, D. W.; Marziali, A.; Bayley, H.; Benner, S. A.; Butler, T.; Di Ventra, M.; Garaj, S.; Hibbs, A.; Huang, X.; *et al*. The Potential and Challenges of Nanopore Sequencing. *Nat. Biotechnol.* **2008**, *26*, 1146–1153.
7. Wickner, W.; Schekman, R. Protein Translocation across Biological Membranes. *Science* **2005**, *310*, 1452–1456.
8. Harsman, A.; Krüger, V.; Bartsch, P.; Honigmann, A.; Schmidt, O.; Rao, S.; Meisinger, C.; Wagner, R. Protein Conducting Nanopores. *J. Phys.: Condens. Matter* **2010**, *22*, 454102–454102.
9. Fèvre, F.; Chich, J. F.; Lauquin, G. J.; Henry, J. P.; Thieffry, M. Comparison of Mitochondrial Cationic Channels in Wild-Type and Porin-Deficient Mutant Yeast. *FEBS Lett.* **1990**, *262*, 201–204.
10. Hill, K.; Model, K.; Ryan, M.; Dietmeier, K.; Martin, F. Tom40 Forms the Hydrophilic Channel of the Mitochondrial Import Pore for Preproteins. *Nature* **1998**.
11. Simon, S. M.; Blobel, G. A Protein-Conducting Channel in the Endoplasmic Reticulum. *Cell* **1991**, *65*, 371–380.
12. Rapoport, T. A. Protein Translocation across the Eukaryotic Endoplasmic Reticulum and Bacterial Plasma Membranes. *Nature* **2007**, *450*, 663–669.
13. Zimmerberg, J.; Parsegian, V. A. Polymer Inaccessible Volume Changes during Opening and Closing of a Voltage-Dependent Ionic Channel. *Nature* **1986**, *323*, 36–39.
14. Oukhaled, G.; Mathe, J.; Biance, A. L.; Bacri, L.; Betton, J.-M.; Lairez, D.; Pelta, J.; Auvray, L. Unfolding of Proteins and Long Transient Conformations Detected by Single Nanopore Recording. *Phys. Rev. Lett.* **2007**, *98*, 158101.
15. Payet, L.; Martinho, M.; Pastoriza-Gallego, M.; Betton, J.-M.; Auvray, L.; Pelta, J.; Mathé, J. Thermal Unfolding of Proteins Probed at the Single Molecule Level Using Nanopores. *Anal. Chem.* **2012**, *84*, 4071–4076.
16. Stefureac, R.; Waldner, L.; Howard, P.; Lee, J. Nanopore Analysis of a Small 86-Residue Protein. *Small* **2008**, *4*, 59–63.
17. Baran, C.; Smith, G. S. T.; Bamm, V. V.; Harauz, G.; Lee, J. S. Divalent Cations Induce a Compaction of Intrinsically Disordered Myelin Basic Protein. *Biochem. Biophys. Res. Commun.* **2010**, *391*, 224–229.
18. Wang, H.-Y.; Ying, Y.-L.; Li, Y.; Kraatz, H.-B.; Long, Y.-T. Nanopore Analysis of B-Amyloid Peptide Aggregation Transition Induced by Small Molecules. *Anal. Chem.* **2011**, *83*, 1746–1752.
19. Sutherland, T.; Long, Y.; Stefureac, R. Structure of Peptides Investigated by Nanopore Analysis. *Nano Lett.* **2004**, *4*, 1273–1277.
20. Meng, H.; Detillieux, D.; Baran, C.; Krasniqi, B.; Christensen, C.; Madampage, C.; Stefureac, R. I.; Lee, J. S. Nanopore Analysis of Tethered Peptides. *J. Pept. Sci.* **2010**, *16*, 701–708.
21. Movileanu, L.; Schmittschmitt, J. P.; Scholtz, J. M.; Bayley, H. Interactions of Peptides with a Protein Pore. *Biophys. J.* **2005**, *89*, 1030–1045.

22. Stefureac, R.; Long, Y.; Kraatz, H.; Howard, P. Transport of A-Helical Peptides through A-Hemolysin and Aerolysin Pores. *Biochemistry* **2006**, *45*, 9172–9179.
23. Pastoriza-Gallego, M.; Rabah, L.; Gibrat, G.; Thiebot, B.; van der Goot, F. G.; Auvray, L.; Betton, J.-M.; Pelta, J. Dynamics of Unfolded Protein Transport through an Aerolysin Pore. *J. Am. Chem. Soc.* **2011**, *133*, 2923–2931.
24. Mahendran, K. R.; Romero-Ruiz, M.; Schlösinger, A.; Winterhalter, M.; Nussberger, S. Protein Translocation through Tom40: Kinetics of Peptide Release. *Biophys. J.* **2012**, *102*, 39–47.
25. Pastoriza-Gallego, M.; Oukhaled, G.; Mathé, J.; Thiebot, B.; Betton, J.-M.; Auvray, L.; Pelta, J. Urea Denaturation of Alpha-Hemolysin Pore Inserted in Planar Lipid Bilayer Detected by Single Nanopore Recording: Loss of Structural Asymmetry. *FEBS Lett.* **2007**, *581*, 3371–3376.
26. Lesieur, C.; Frutiger, S.; Hughes, G.; Kellner, R.; Pattus, F.; van der Goot, F. G. Increased Stability upon Heptamerization of the Pore-Forming Toxin Aerolysin. *J. Biol. Chem.* **1999**, *274*, 36722–36728.
27. Niedzwiecki, D. J.; Grazul, J.; Movileanu, L. Single-Molecule Observation of Protein Adsorption onto an Inorganic Surface. *J. Am. Chem. Soc.* **2010**, *132*, 10816–10822.
28. Firnkes, M.; Pedone, D.; Knezevic, J. Electrically Facilitated Translocations of Proteins through Silicon Nitride Nanopores: Conjoint and Competitive Action of Diffusion, Electrophoresis, and Electroosmosis. *Nano Lett.* **2010**, *10*, 2162–2167.
29. Yusko, E. C.; Johnson, J. M.; Majd, S.; Prangkio, P.; Rollings, R. C.; Li, J.; Yang, J.; Mayer, M. Controlling Protein Translocation through Nanopores with Bio-Inspired Fluid Walls. *Nat. Nanotechnol.* **2011**, *6*, 253–260.
30. Talaga, D. S.; Li, J. Single-Molecule Protein Unfolding in Solid State Nanopores. *J. Am. Chem. Soc.* **2009**, *131*, 9287–9297.
31. Han, A.; Schürmann, G. S.; Mondin, G.; Bitterli, R. A.; Hegelbach, N. G.; de Rooij, N. F.; Staufer, U. Sensing Protein Molecules Using Nanofabricated Pores. *Appl. Phys. Lett.* **2006**, *88*, 093901.
32. Han, A.; Creus, M.; Schürmann, G.; Linder, V. Label-Free Detection of Single Protein Molecules and Protein−Protein Interactions Using Synthetic Nanopores. *Anal. Chem.* **2008**, *80*, 4651–4658.
33. Freedman, K. J.; Jürgens, M.; Prabhu, A.; Ahn, C. W.; Jemth, P.; Edel, J. B.; Kim, M. J. Chemical, Thermal, and Electric Field Induced Unfolding of Single Protein Molecules Studied Using Nanopores. *Anal. Chem.* **2011**, *83*, 5137–5144.
34. Wei, R.; Gatterdam, V.; Wieneke, R.; Tampé, R.; Rant, U. Stochastic Sensing of Proteins with Receptor-Modified Solid-State Nanopores. *Nat. Nanotechnol.* **2012**, *7*, 257–263.
35. Fologea, D.; Ledden, B.; McNabb, D. S.; Li, J. Electrical Characterization of Protein Molecules by a Solid-State Nanopore. *Appl. Phys. Lett.* **2007**, *91*, nihpa38991.
36. Sexton, L. T.; Horne, L. P.; Sherrill, S. A.; Bishop, G. W.; Baker, L. A.; Martin, C. R. Resistive-Pulse Studies of Proteins and Protein/Antibody Complexes Using a Conical Nanotube Sensor. *J. Am. Chem. Soc.* **2007**, *129*, 13144–13152.
37. Sexton, L. T.; Mukaibo, H.; Katira, P.; Hess, H.; Sherrill, S. A.; Horne, L. P.; Martin, C. R. An Adsorption-Based Model for Pulse Duration in Resistive-Pulse Protein Sensing. *J. Am. Chem. Soc.* **2010**, *132*, 6755–6763.
38. Ammenti, A.; Cecconi, F.; Marconi, U. M. B.; Vulpiani, A. A Statistical Model for Translocation of Structured Polypeptide Chains through Nanopores. *J. Phys. Chem. B* **2009**, *113*, 10348–10356.
39. Bacci, M.; Chinappi, M.; Casciola, C. M.; Cecconi, F. Role of Denaturation in Maltose Binding Protein Translocation Dynamics. *J. Phys. Chem. B* **2012**, *116*, 4255–4262.
40. Makarov, D. Computer Simulations and Theory of Protein Translocation. *Acc. Chem. Res.* **2008**, *42*, 281–289.
41. Raffy, S.; Sassoon, N.; Hofnung, M.; Betton, J.-M. Tertiary Structure-Dependence of Misfolding Substitutions in Loops of the Maltose-Binding Protein. *Protein Sci.* **1998**, *7*, 2136–2142.
42. Oukhaled, A.; Cressiot, B.; Bacri, L.; Pastoriza-Gallego, M.; Betton, J.-M.; Bourhis, E.; Jede, R.; Gierak, J.; Auvray, L.; Pelta, J. Dynamics of Completely Unfolded and Native Proteins through Solid-State Nanopores as a Function of Electric Driving Force. *ACS Nano* **2011**, *5*, 3628–3638.
43. Ghosal, S. Electrophoresis of a Polyelectrolyte through a Nanopore. *Phys. Rev. E* **2006**, *74*, 041901.
44. Ghosal, S. Effect of Salt Concentration on the Electrophoretic Speed of a Polyelectrolyte through a Nanopore. *Phys. Rev. Lett.* **2007**, *98*, 238104.
45. van Dorp, S.; Keyser, U. F.; Dekker, N. H. A. D. C.; Lemay, S. G. Origin of the Electrophoretic Force on DNA in Solid-State Nanopores. *Nat. Phys.* **2009**, *5*, 347–351.
46. Keyser, U. F.; van Dorp, S.; Lemay, S. G. Tether Forces in DNA Electrophoresis. *Chem. Soc. Rev.* **2010**, *39*, 939–947.
47. Cruz-Chu, E. R.; Aksimentiev, A.; Schulten, K. Ionic Current Rectification through Silica Nanopores. *J. Phys. Chem. C* **2009**, *113*, 1850–1862.
48. Muthukumar, M. *Polymer Translocation*; CRC Press, 2009.
49. Ho, C.; Qiao, R.; Heng, J. B.; Chatterjee, A.; Timp, R. J.; Aluru, N. R.; Timp, G. Electrolytic Transport through a Synthetic Nanometer-Diameter Pore. *Proc. Natl. Acad. Sci. U. S. A.* **2005**, *102*, 10445–10450.
50. Kowalczyk, S. W.; Kapinos, L.; Blosser, T. R.; Magalhães, T.; van Nies, P.; Lim, R. Y. H.; Dekker, C. Single-Molecule Transport across an Individual Biomimetic Nuclear Pore Complex. *Nat. Nanotechnol.* **2011**, *6*, 433–438.
51. Krapf, D.; Wu, M. Y.; Smeets, R. M. M.; Zandbergen, H. W.; Dekker, C.; Lemay, S. G. Fabrication and Characterization of Nanopore-Based Electrodes with Radii Down to 2 nm. *Nano Lett.* **2006**, *6*, 105–109.
52. Bacri, L.; Oukhaled, A. G.; Schiedt, B.; Patriarche, G.; Bourhis, E.; Gierak, J.; Pelta, J.; Auvray, L. Dynamics of Colloids in Single Solid-State Nanopores. *J. Phys. Chem. B* **2011**, *115*, 2890–2898.
53. Siwy, Z.; Fulinski, A. Fabrication of a Synthetic Nanopore Ion Pump. *Phys. Rev. Lett.* **2002**, *89*, 198103.
54. Kim, M.; McNally, B.; Murata, K. Characteristics of Solid-State Nanometre Pores Fabricated Using a Transmission Electron Microscope. *Nanotechnology* **2007**.
55. Hall, J. E. Access Resistance of a Small Circular Pore. *J. Gen. Physiol.* **1975**, *66*, 531–532.
56. Pedone, D.; Firnkes, M.; Rant, U. Data Analysis of Translocation Events in Nanopore Experiments. *Anal. Chem.* **2009**, *81*, 9689–9694.
57. Muthukumar, M. Theory of Capture Rate in Polymer Translocation. *J. Chem. Phys.* **2010**, *132*, 195101.
58. Muthukumar, M. Polymer Escape through a Nanopore. *J. Chem. Phys.* **2003**, *118*, 5174.
59. Brochard, F.; de Gennes, P. G. Dynamics of Confined Polymer-Chains. *J. Chem. Phys.* **1977**, *67*, 52–56.
60. Wanunu, M.; Morrison, W.; Rabin, Y.; Grosberg, A. Y.; Meller, A. Electrostatic Focusing of Unlabelled DNA into Nanoscale Pores Using a Salt Gradient. *Nat. Nanotechnol.* **2009**.
61. Roach, P.; Farrar, D.; Perry, C. C. Interpretation of Protein Adsorption: Surface-Induced Conformational Changes. *J. Am. Chem. Soc.* **2005**, *127*, 8168–8173.
62. Zhang, J.; Shklovskii, B. I. Effective Charge and Free Energy of DNA Inside an Ion Channel. *Phys. Rev. E Stat. Nonlin. Soft Matter Phys.* **2007**, *75*, 021906.
63. Ghosal, S. Electrokinetic-Flow-Induced Viscous Drag on a Tethered DNA inside a Nanopore. *Phys. Rev. E* **2007**, *76*, 061916.
64. de Gennes, P.-G.; *et al.* Flexible Polymers in Nanopores. *Polym. Confined Environ.* **1999**, *138*, 91–105.
65. Gibrat, G.; Pastoriza-Gallego, M.; Thiebot, B.; Breton, M.-F.; Auvray, L.; Pelta, J. Polyelectrolyte Entry and Transport through an Asymmetric Alpha-Hemolysin Channel. *J. Phys. Chem. B* **2008**, *112*, 14687–14691.
66. Arie, J.-P.; Miot, M.; Sassoon, N.; Betton, J.-M. Formation of Active Inclusion Bodies in the Periplasm of Escherichia Coli. *Mol. Microbiol.* **2006**, *62*, 427–437.
67. Brun, L.; Pastoriza-Gallego, M.; Oukhaled, G.; Mathe, J.; Bacri, L.; Auvray, L.; Pelta, J. Dynamics of Polyelectrolyte Transport through a Protein Channel as a Function of Applied Voltage. *Phys. Rev. Lett.* **2008**, *100*.